

Superconductivity and the Pseudogap in the two-dimensional Hubbard model

Emanuel Gull,^{1,2*} Olivier Parcollet,³ Andrew J. Millis²

¹Max Planck Institut für Physik komplexer Systeme, Dresden, Germany

²Department of Physics, Columbia University, New York, NY, USA

³Institut de Physique Théorique, CEA, IPhT, CNRS, URA 2306, F-91191 Gif-sur-Yvette, France

*To whom correspondence should be addressed; E-mail: gull@pks.mpg.de.

Lamellar perovskite-based copper oxide compounds display three remarkable properties: *d*-wave superconductivity, with unprecedentedly high transition temperatures (1), a nontrivial (‘Mott’) insulating state (2) and a ‘pseudogap’ regime of suppressed density of states (3). P. W. Anderson (2) argued that these have a common origin as strong-correlation phenomena that could be understood in terms of the two-dimensional Hubbard model, but the interplay between the pseudogap and the superconductivity has remained controversial, with some authors suggesting the pseudogap is a signature of unusual superconducting fluctuations (4, 5) and others suggesting it is a competing phase or regime (3, 6). Here we use new numerical techniques (7, 8) to solve the Hubbard model in the dynamical cluster approximation (9), which becomes exact as cluster size tends to infinity. Our methods enable the study of interactions strong enough and temperatures low enough to that the properties of the superconducting state and its relation to the Mott insulator and the pseudogap can be determined for clusters large enough to be representative of the thermodynamic limit and show that in the Hubbard model the two phenomena,

while both linked to proximity to the Mott insulating state, are competing phenomena. Superconductivity is found to occur in a dome separated from the Mott insulating state by the pseudogap. The emergence of superconductivity from the pseudogap regime leads to a decrease in the gap (i.e. the creation of new states within the pseudogap), in agreement with recent angle-resolved photoemission data (10).

Determining the properties of the superconducting state of the two dimensional Hubbard model, defined as

$$H = \sum_{p,\sigma} (\epsilon_p - \mu) c_{p,\sigma}^\dagger c_{p,\sigma} + U \sum_i n_{i,\uparrow} n_{i,\downarrow}, \quad (1)$$

has been a central issue in condensed matter theory. The existence of a superconducting state was suggested by numerical and analytic studies of superconducting correlations in related one-dimensional “ladder” systems (11). This idea was supported by analytic calculations, originally perturbatively about suitably defined weak coupling limits (12) and later improved by renormalization group methods (13). Early attempts to access the superconducting phase numerically led to inconsistent results (14–17), but the development of cluster dynamical mean field (DMFT) methods, which become exact as cluster size $N_c \rightarrow \infty$, (9) provided a new approach. In pioneering papers Lichtenstein and Katsnelson (18) and Maier *et al.* (19) showed that these methods lead to d -wave superconductivity in four-site cluster approximations. Further studies of the superconducting state of four site clusters were performed (20–23), but we now know (9, 20, 24) that the four-site cluster is in many respects an outlier, both because the isolated four site cluster (but not larger clusters) has an RVB singlet ground state which dominates the physical properties and because the four site cluster lacks the momentum resolution needed to exhibit the sector selective transition which is the expression of the pseudogap in this model (24). Landmark studies of the pairing susceptibility of larger clusters performed by Maier and collaborators (25) demonstrated that $d_{x^2-y^2}$ superconductivity is a property of the infinite cluster size limit. However, up to now the superconducting properties of these larger

clusters have been studied only at weak coupling (where the pseudogap phase was not present) and via analysis of the normal state pairing susceptibility (which precludes analysis of the superconducting state) (25, 26) so the question of the interplay of the pseudogap, the Mott phase and the superconductivity has remained open.

Our studies use the dynamical cluster approximation (DCA) version of dynamical mean field theory (9). We use electron dispersion $\epsilon_p = -2t [\cos(p_x) + \cos(p_y)] - 4t' \cos(p_x) \cos(p_y)$ (with the t' permitting a breaking of particle-hole symmetry). We study a range of interactions $0 < U < 7t$ and temperatures as low as $t/60$, enabling access to the low- T properties of the superconducting state and to interactions strong enough to drive a Mott transition. Submatrix update techniques (7) are crucial; also, in some parameter regimes care is required in converging to the superconducting state (see supplementary material). We present results for clusters with $N_c = 4, 8, 16$ sites, large enough to distinguish generic behavior from that specific to particular clusters (24).

We study the paramagnetic phase of the model, allowing for all possible spin singlet superconducting order parameters. Consistently across all clusters and in agreement with previous results (12, 13, 25) we found that the Hubbard model possesses a d-wave superconducting state, with a typical transition temperature $\sim t/40 \approx 100K$ (using a $t \approx 0.3eV$ representative of the CuO_2 superconductors). At the temperatures accessible to us, superconductivity occurs only for interactions larger than a critical value and dopings sufficiently close ($\lesssim 20\%$) to half filling, but persists up to the largest interactions ($U/t = 8$) we have investigated.

The right panel of Fig. 1 presents the phase diagram determined from a comprehensive survey of parameter space for $N_c = 8$, which previous work (24) shows adequately represents the normal state physics of the model. Studies of selected U and doping values in the computationally much more expensive $N_c = 16$ site cluster confirm that the physics found for $N_c = 8$ is generic. The phase diagram in the absence of superconductivity has been determined (24). One

key feature is the presence of a fully gapped (“Mott”) insulating phase for density $n = 1$ and $U > U_c \approx 6t$ indicated by the vertical heavy green line. The Mott phase is separated from the normal Fermi-liquid phase by a pseudogap regime characterized by a suppression of density of states near the $(0, \pi), (\pi, 0)$ regions of the Brillouin zone, with states near the zone diagonal remaining unaffected. The onset of the normal state pseudogap is indicated by the dashed purple line in Fig. 1.

The red shaded region in Fig. 1 indicates the parameters where superconductivity is found: at the temperatures accessible to us it ‘turns on’ as the pseudogap regime is approached, is strongest at the normal state pseudogap boundary, and is suppressed as parameters are tuned deeper into the normal state pseudogap regime. The superconducting regime is separated from the Mott insulating state by a non-superconducting pseudogapped regime (blue shaded region in Fig. 1). The same physics is found if interaction strength is varied at doping $n = 1$. The lower left panel shows the strength of the superconducting order parameter as a function of interaction strength. Although the critical interaction strength for superconductivity onset varies with cluster size, in the larger clusters the superconductivity is tied to the vicinity of the pseudogap.

The situation is somewhat different in the four site cluster, which lacks the momentum resolution to exhibit the momentum-space dependent density of states suppression which is the essence of the pseudogap phenomenon (24). In this cluster superconductivity extends all the way to the boundary of the Mott phase as shown in the upper left panel of Fig. 1.

Fig. 2 presents the superconducting transition temperature and gap values estimated as described in the supplementary material. The transition temperature also has a dome-like behavior, with the highest transition temperature occurring near the onset of the normal state pseudogap (insets of Fig. 2), whereas the gap monotonically increases from high to low doping or low to high interaction. We find $2\Delta/T_c \sim 7.5 - 8$ in the region outside the pseudogap (about twice as large as the BCS value $2\Delta/T_c \simeq 3.5$), and becoming rapidly larger within the pseudogap

regime as the endpoint of the superconducting regime is approached. Note in particular that the superconducting transition temperature and anomalous expectation value (see inset to Fig. 1) vanish for a range of $U < U_{Mott}$ even though the gap continues to increase up to the endpoint of the superconducting phase.

Fig. 3 presents the frequency and temperature dependence of the density of states. The upper panel shows spectra representative of dopings higher than, or interactions weaker than, the values which maximize T_c , so that superconductivity emerges from a relatively conventional normal state. The spectra are consistent with expectations from standard theory (29): the onset of superconductivity is associated with a suppression of density of states at low frequency and with the formation of density of states (“coherence”) peaks at slightly higher energies. We define the superconducting gap as half of the peak to peak distance. The behavior is conventional in the sense that the area in the coherence peaks comes mainly from the states removed at $|\omega| < \Delta$ (see further discussion in the supplementary material). The gap amplitude develops very rapidly with temperature: only at the temperature closest to T_c is the peak to peak splitting appreciably different from its value at the lowest T .

The situation is quite different when superconductivity emerges from the pseudogap regime. Representative spectra are shown in the lower panel of Fig. 3. The normal state pseudogap is visible at $T > T_c$ as a suppression of the density of states at low frequencies with a broad gap structure at higher frequencies. The normal state pseudogap maxima are marked by dashed lines. The development of superconductivity is characterized by the formation of coherence peaks at energies *below* the pseudogap, i.e. by a *decrease* in gap magnitude as the superconducting state is entered. Furthermore, most (typically more than 50%) of the spectral weight in the coherence peak is drawn from frequencies greater than the superconducting gap energies. Finally, as shown in Fig. 2, the superconducting gap in this regime remains large although the transition temperature is driven to 0. This behavior is consistent with recent experimental

reports (10) that in underdoped cuprates the emergence of superconductivity out of the pseudogap regime is associated with the formation of new states at energies lower than the pseudogap energy and that the superconducting gap is tied to the pseudogap.

Insight into the frequency scales relevant to the pairing interaction comes from the imaginary part of the real-axis anomalous self-energy shown in Fig. 4. Within our numerical precision the only important structure is a sharp peak at the very low frequency $\Omega_p \approx 0.15t$. This scale is found for all of the parameters we have examined, and is consistent with a spin-fluctuation origin for the superconductivity (26). We have not found evidence for the contribution from higher frequency ($\omega \sim U$) scales reported by Ref. (22) (see also (30)). The difference may arise from the different interaction values studied, from the precision of our real frequency spectra or from the special properties of the four-site cluster, for which the frequency scale is clearly larger (see supplementary material).

The existence of $d_{x^2-y^2}$ superconductivity in the Hubbard model has been previously established. We find, robustly over a range of cluster sizes, interaction strengths, and carrier concentrations, that the superconducting phase occurs within a superconducting dome bounded on one side by proximity to the Mott insulating phase and on the other by the weak coupling/large doping regime. Superconductivity is characterized by a low pairing energy scale, is maximized in the vicinity of the pseudogap onset but competes with the pseudogap and is driven to zero deep within the pseudogap regime. When superconductivity emerges from the pseudogap regime it fundamentally reconstructs the density of states, leading in particular to new states within the pseudogap.

Our methods are restricted (at least in the present state of development) to models with local density-density interactions and to situations where the fermionic sign problem, which gets exponentially worse with increasing cluster size and decreasing T , is not too severe. In the context of the two-dimensional Hubbard model the practical restriction is to $N_c \lesssim 16$ and inter-

action $U \lesssim 7$. These values are large enough to enable access to the doped Mott phase. Within these constraints, investigations of the effect of second neighbor coupling, of the frequency dependence of the anomalous self energy, and of the two particle (e.g. Raman) spectra should be feasible. Also, a significant difference between our calculations and experiment is that we find a larger anomalous Green function on the electron doped side. Inclusion of long-ranged antiferromagnetism and also extension of our results to the ‘three-band’ copper oxide models is needed to understand these issues further.

Acknowledgments We acknowledge helpful discussions with Thomas Maier and Michel Ferrero. AJM and EG were supported by NSF-DMR-1006282. This research used resources of GENCI-CCRT (Grant No. 2011- t2011056112) and of the National Energy Research Scientific Computing Center, which is supported by the Office of Science of the U.S. Department of Energy under Contract No. DE-AC02-05CH11231. A portion of this research was conducted at the Center for Nanophase Materials Sciences, which is sponsored at Oak Ridge National Laboratory by the Office of Basic Energy Sciences, U.S. Department of Energy.

Author Contributions All authors contributed to the design of the study, creation of the algorithm, data analysis, and manuscript preparation. The computer code was written and simulation data were produced by E.G.

References and Notes

1. J. G. Bednorz, K. A. Müller, *Zeitschrift für Physik B Condensed Matter* **64**, 189 (1986). 10.1007/BF01303701.
2. P. W. ANDERSON, *Science* **235**, 1196 (1987).
3. S. Hüfner, M. A. Hossain, A. Damascelli, G. A. Sawatzky, *Reports on Progress in Physics* **71**, 062501 (2008).

4. V. J. Emery, S. A. Kivelson, *Nature* pp. 434 – 437 (1995).
5. Y. Wang, *et al.*, *Phys. Rev. Lett.* **88**, 257003 (2002).
6. L. Taillefer, *Annual Review of Condensed Matter Physics* **1**, 51 (2010).
7. E. Gull, *et al.*, *Phys. Rev. B* **83**, 075122 (2011).
8. E. Gull, *et al.*, *Rev. Mod. Phys.* **83**, 349 (2011).
9. T. Maier, M. Jarrell, T. Pruschke, M. H. Hettler, *Rev. Mod. Phys.* **77**, 1027 (2005).
10. R.-H. He, *et al.*, *Science* **331**, 1579 (2011).
11. E. Dagotto, T. M. Rice, *Science* **271**, 618 (1996).
12. D. Zanchi, H. J. Schulz, *Phys. Rev. B* **54**, 9509 (1996).
13. C. J. Halboth, W. Metzner, *Phys. Rev. Lett.* **85**, 5162 (2000).
14. D. J. Scalapino, S. R. White, S. C. Zhang, *Phys. Rev. Lett.* **68**, 2830 (1992).
15. F. F. Assaad, W. Hanke, D. J. Scalapino, *Phys. Rev. Lett.* **71**, 1915 (1993).
16. S. Zhang, J. Carlson, J. E. Gubernatis, *Phys. Rev. Lett.* **74**, 3652 (1995).
17. S. Sorella, *et al.*, *Phys. Rev. Lett.* **88**, 117002 (2002).
18. A. I. Lichtenstein, M. I. Katsnelson, *Phys. Rev. B* **62**, R9283 (2000).
19. T. Maier, M. Jarrell, T. Pruschke, J. Keller, *Phys. Rev. Lett.* **85**, 1524 (2000).
20. K. Haule, *Phys. Rev. B* **75**, 155113 (2007).
21. M. Civelli, *et al.*, *Phys. Rev. Lett.* **100**, 046402 (2008).

- 22. T. A. Maier, D. Poilblanc, D. J. Scalapino, *Phys. Rev. Lett.* **100**, 237001 (2008).
- 23. S. S. Kancharla, *et al.*, *Phys. Rev. B* **77**, 184516 (2008).
- 24. E. Gull, M. Ferrero, O. Parcollet, A. Georges, A. J. Millis, *Phys. Rev. B* **82**, 155101 (2010).
- 25. T. A. Maier, M. Jarrell, T. C. Schulthess, P. R. C. Kent, J. B. White, *Phys. Rev. Lett.* **95**, 237001 (2005).
- 26. T. A. Maier, M. S. Jarrell, D. J. Scalapino, *Phys. Rev. Lett.* **96**, 047005 (2006).
- 27. P. Werner, E. Gull, O. Parcollet, A. J. Millis, *Phys. Rev. B* **80**, 045120 (2009).
- 28. E. Gull, O. Parcollet, P. Werner, A. J. Millis, *Phys. Rev. B* **80**, 245102 (2009).
- 29. J. Bardeen, L. N. Cooper, J. R. Schrieffer, *Phys. Rev.* **108**, 1175 (1957).
- 30. B. Kyung, D. Sénéchal, A.-M. S. Tremblay, *Phys. Rev. B* **80**, 205109 (2009).

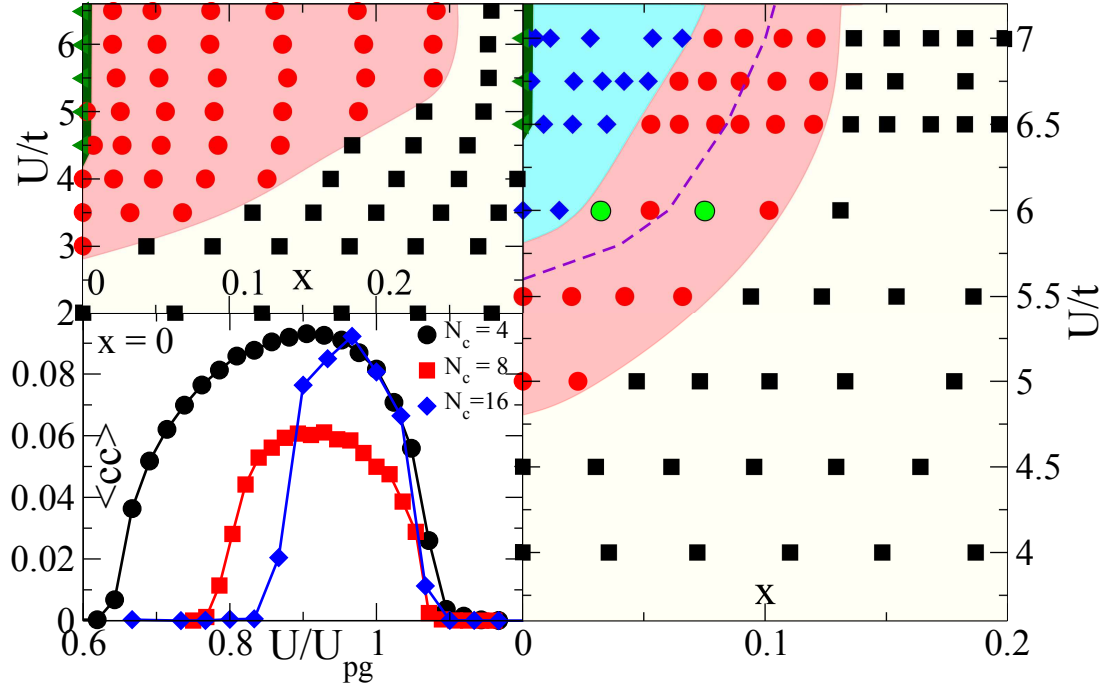


Figure 1: **Superconducting phase diagram of the two-dimensional Hubbard model** in plane of interaction strength U and carrier concentration x computed using the 8-site (right panel) and 4-site (left upper panel) DCA dynamical mean field approximation at temperature $T = t/40$ with $t'/t = 0$. Dashed line: location of the normal state pseudogap onset. Circles (red and light green) and red shading indicates the superconducting region, squares (black) and no shading the non-superconducting Fermi liquid, diamonds (blue) and blue shading the nonsuperconducting pseudogap region (eight-site only, right panel) and triangles and heavy solid line (dark green) the Mott insulating region at $n = 1$ and $U > U_c$. Light green circles denote the points analyzed in Fig. 3. Lower left panel: Anomalous equal-time correlator $\langle c_{K=(\pi,0)}^\dagger c_{K=(-\pi,0)} \rangle$ as a function of interaction for clusters of size $N_c = 4, 8, 16$, as a function of U/U_{pg} . Dashed line and pseudogap scale $U_{pg} = 4.2$ (4-site, circles), 5.6 (8-site, squares), and 3 (16-site, diamonds) determined as in (24, 27, 28).

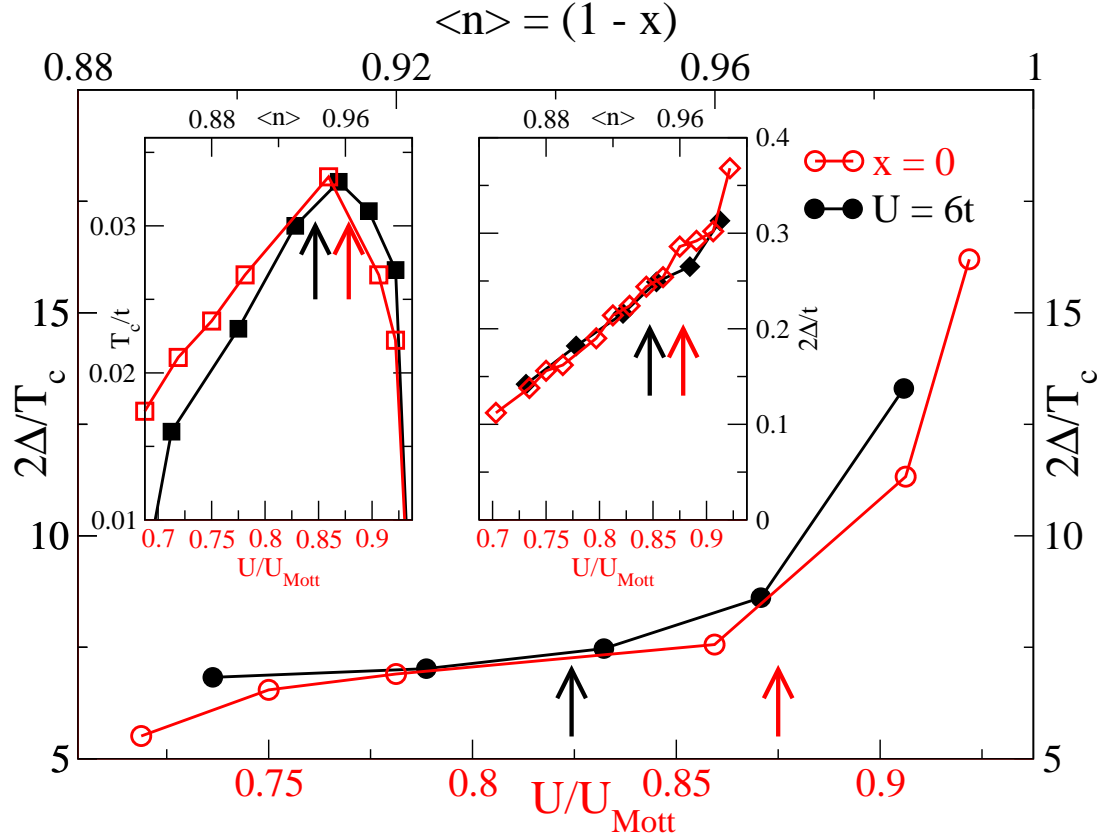


Figure 2: **Gap to transition temperature ratio** $2\Delta/T_c$ (main panel) computed using the 8-site DCA approximation both by varying U at $x = 0$ (open symbols, lower axis, red color, $U_{Mott} = 6.4t$) and by varying x for $U = 6t$ (filled symbols, upper axis, black). Left inset, squares: doping and interaction dependence of transition temperature for same parameters, showing superconducting dome. Right inset, diamonds: doping and interaction dependence of gap $2\Delta/t$. Arrows: onset of normal state pseudogap.

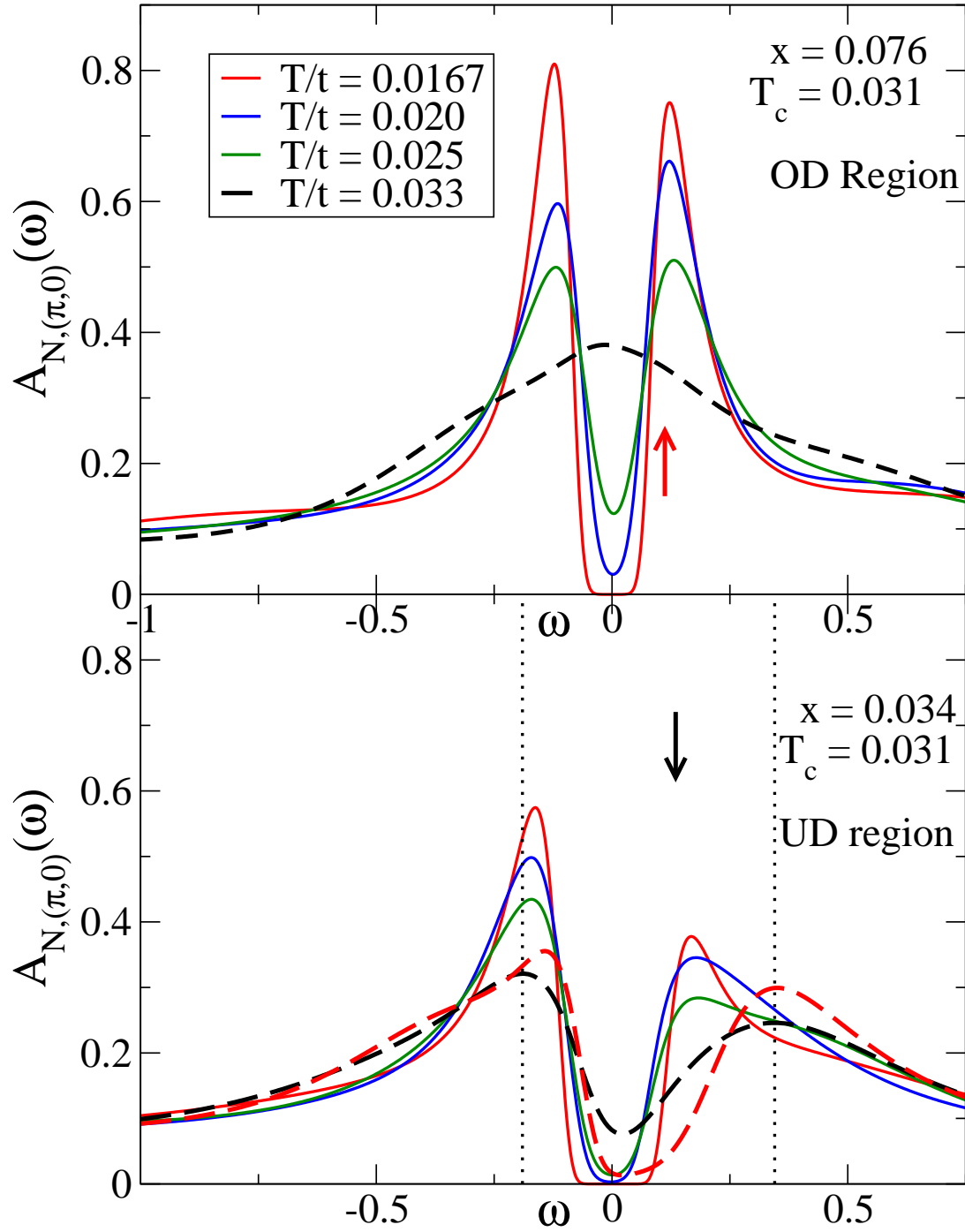


Figure 3: **Analytically continued spectral function** computed at $U = 6t$ for antinodal sector showing temperature evolution of gap structure for a typical optimally doped / overdoped state ($x = 0.076$, upper panel) and underdoped pseudogap state ($x = 0.034$, lower panel). Solid lines: superconducting spectral function. Dashed lines: normal state spectral function, obtained for $T = t/60$ by artificially suppressing superconductivity. Arrows: superconducting gap size Δ . Dotted lines: pseudogap size at $T = t/30$ (obtained from maximum in spectral function).

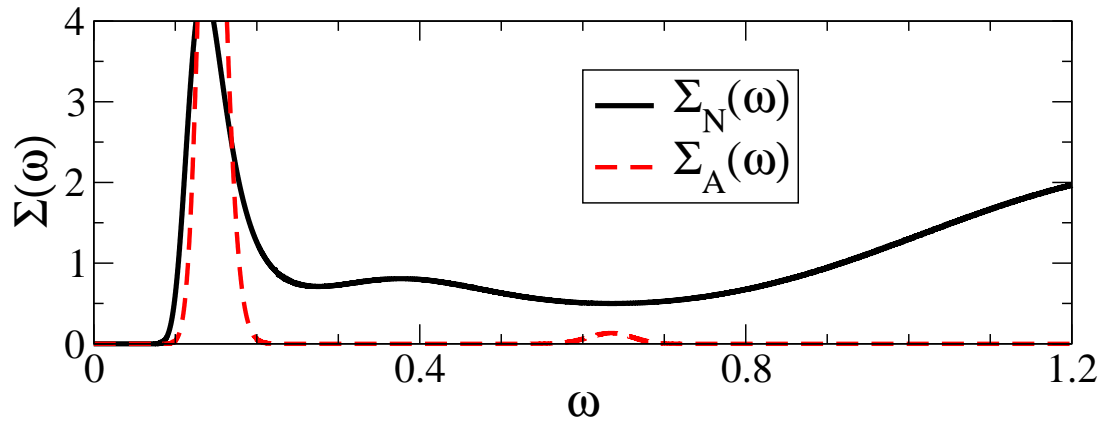


Figure 4: **Imaginary part of self energy** calculated for particle-hole symmetric Hubbard model at $n = 1$, $U = 5.8$, and $T = t/60$ obtained by directly continuing the Matsubara axis self energy. Normal component: black solid line. Anomalous component: dashed red line.

Supplementary Material: Superconductivity and the Pseudogap in the two-dimensional Hubbard model

Emanuel Gull,^{1,2*} Olivier Parcollet,³ Andrew J. Millis²

¹Max Planck Institut für Physik komplexer Systeme, Dresden, Germany

²Department of Physics, Columbia University, New York, NY, USA

³Institut de Physique Théorique, CEA, IPhT, CNRS, URA 2306, F-91191 Gif-sur-Yvette, France

*To whom correspondence should be addressed; E-mail: gull@pks.mpg.de.

July 12, 2012

1 Numerical procedure

1.1 Method

We study the two dimensional Hubbard model (Eq. 1 of main text) using the dynamical cluster approximation (DCA) version of cluster dynamical mean field theory (*I*), with our recent implementation of a Nambu (superconducting-state) version of the numerically exact continuous-time auxiliary field (14, 24) quantum impurity solver with submatrix updates (25) based on the open source ALPS (2–4) libraries.

To describe the DMFT self-consistency process it is convenient to use the Nambu matrix notation introducing Pauli matrices $\tau_{0,1,2,3}$ in particle-hole space so that the Green function \mathbf{G} , self energy Σ and mean field function \mathcal{G}_0^{-1} have normal (N) and anomalous (A) components (e.g. $\Sigma = \tau_0 \Sigma_N + \tau_1 \Sigma_A$). The mean field function is determined from

$$\mathcal{G}_0^{-1}(K, i\omega_n) = \Sigma(K, i\omega_n) + \frac{N_c}{N} \left[\sum_{k \in K} \mathbf{G}_{latt}(k, i\omega_n) \right]^{-1} \quad (1)$$

with

$$\mathbf{G}_{latt}(k, i\omega_n) = [i\omega_n \tau_0 + (\mu - \epsilon_k) \tau_3 - \Sigma(K, i\omega_n)]^{-1} \quad (2)$$

Here K labels momentum sectors and Σ is obtained from a solution of the corresponding impurity model.

The extension to superconductivity means that all matrices are twice as large as in a normal state computation at the same temperature. The doubling of matrix size means that submatrix update techniques (5) are crucial for accessing the large interaction strengths and low temperatures needed in this study. Critical slowing down means that typically more than 50 iterations are needed to converge near the superconducting phase transition.

1.2 Convergence procedure

Particularly in the pseudogap regime, the onset of superconductivity drastically changes the low energy electronic structure. A consequence is that adding a superconducting component to a converged non-superconducting solutions leads to very slow convergence, and care is required in converging to the superconducting state. We have found that the most stable procedure is to begin at a relatively high temperature (e.g. $\beta = 10/t$) and introduce a pairing field $\eta_1(k) = \eta_1 \phi_k$ via the replacement $\mathbf{G}(k, i\omega_n; \eta_1) = [i\omega_n \tau_0 + (\mu - \epsilon_k) \tau_3 + \eta_1(k) \tau_1 - \Sigma]^{-1}$, with e.g. $\phi_k = \cos k_x - \cos k_y$ for d -wave superconductivity, and η_1 typically 0.1t. Retaining the pairing field we obtain converged solutions $\mathbf{G}(K, i\omega_n; \eta_1)$ first at the initial temperature, then, using the solution at the initial temperature as a seed, at the desired range of lower temperatures. We remark that the sign problem for large η_1 is much less severe than at $\eta = 0$, so these computations are not inordinately expensive.

Then, at each temperature, using the converged $\mathbf{G}(K, i\omega_n; \eta_1)$ as a seed, we set $\eta_1 = 0$ in the self-consistency condition and continue iterating until convergence is reached. At selected points we check the solution by taking the putatively converged self energy, dividing the anomalous part by a large number (typically 20), and verifying that under further iterations the solution converges back to the one previously found.

2 Transition temperatures and gap magnitudes

We estimated the transition temperature by performing a linear extrapolation of the square of the equal-time anomalous Green's function $G_{A,(\pi,0)}$, using the three highest temperatures at which $G_A > 0.1$. We cross-checked the transition temperature estimates by computing the temperature at which the inverse of the normal state pairing susceptibility vanishes.

We obtained the superconducting gap by analytically continuing the $G_N(\tau)$ and reading off the distance between the quasiparticle peaks. We cross-checked the gap values by analytically continuing the self-energies (see below).

The crucial finding, namely that the gap is smaller in the superconducting than in the pseudogap state may be seen directly from our imaginary time data. Eq. 4 implies that

$$\beta G\left(\tau = \frac{\beta}{2}\right) = \int \frac{d\omega}{\pi} \frac{A(\omega)}{4 \cosh \frac{\beta\omega}{2}} \quad (3)$$

In a system with a gap Δ Eq. 3 implies $G(\tau = \beta/2) \sim e^{-\Delta/2T}$. Fig. 1 shows that at $\beta = 60$ and

$U = 5.8t$ the $G(\tau)$ computed with superconductivity suppressed indeed lies lower than that in the superconducting state, indicating that the normal state has a larger gap than superconducting state.

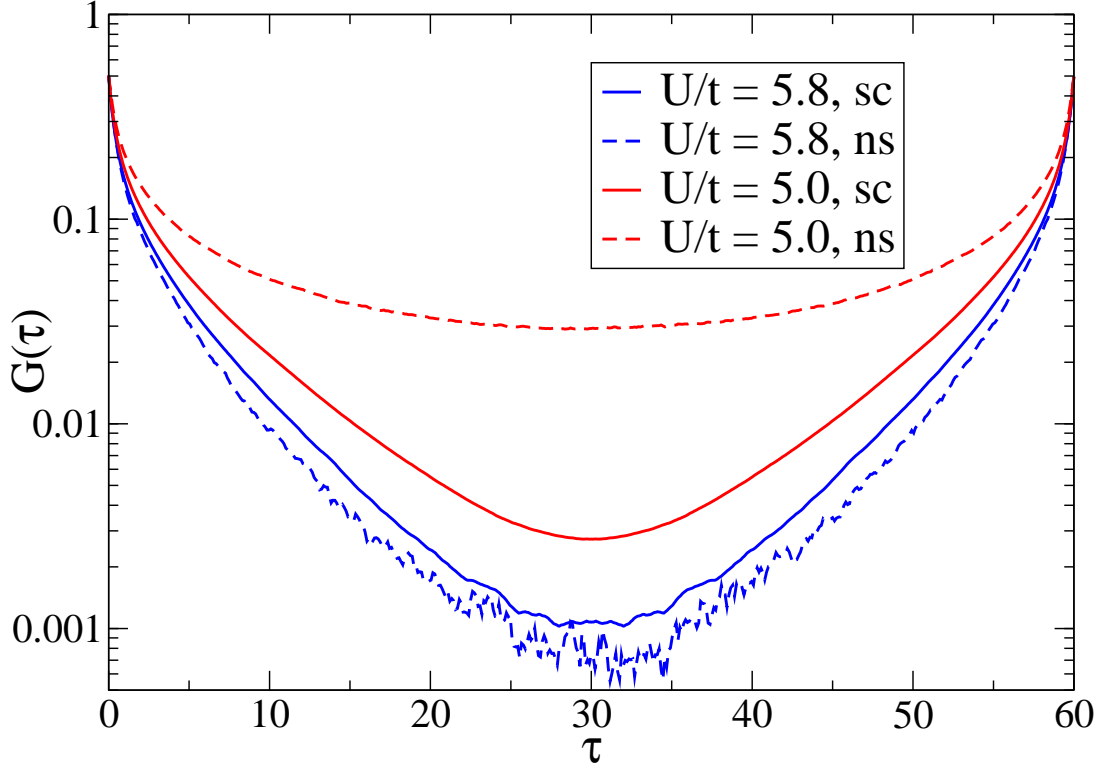


Figure 1: Imaginary time Green function (normal, local component) measured in quantum Monte Carlo procedure for normal states (dashed lines) and superconducting states (solid lines) for $n = 1$ and $U = 5.0t$ (upper traces, red online) and $U = 5.8t$ (lower traces, blue online).

3 Analytic Continuation

3.1 General observations

We perform quantum Monte Carlo calculations, obtaining Green functions and self energies as functions of imaginary time. Densities of states and excitation spectra are obtained by inverting the relation between the imaginary-time Green's function G or self energy Σ and the associated spectral function A (for G) or Σ'' (for Σ) which is

$$G(\tau) = \int_{-\infty}^{\infty} d\omega \frac{e^{-\tau\omega}}{1 + e^{-\beta\omega}} \mathbf{A}(\omega). \quad (4)$$

The inversion of Eq. 4 is an ill-posed problem, because the kernel in Eq. 4 has many very small eigenvalues, so its inverse has many large ones, implying that small (statistical) fluctuations in the input data G cause large fluctuations in A . To find a solution we employ the maximum entropy continuation method (6).

Accurate knowledge of errors in the input data is crucial for a reliable continuation. We estimated these errors from eight consecutive iterations of the converged solution. We assumed the covariance matrix to be diagonal in frequency, based on earlier work in the normal state (7). We assessed the quality of our continuations by verifying that the back-continuation Eq. 4 did not contain systematic deviations from G within the errors bars of the data. Further confidence comes from the fact that the results do not change significantly as the precision is increased and that the change in the spectral functions is gradual and systematic as parameters ($U, T, \langle n \rangle$) are varied. However, uncertainties remain in the continued quantities. Data near $\omega = 0$ are in general more reliable and reproducible than data at high frequencies, and our estimates of energy gaps and of densities of states at frequencies up to $\omega \sim 0.5t$ are robust to choices of model function and input data, and show reasonable trends between calculations. However, the continuations in particular contain small amplitude long-period oscillations which account for part of the differences seen between curves in Fig. 3 of the main text at $\omega \gtrsim 0.5t$ and which complicate for example the problem of obtaining reasonable estimates for the difference between two spectral functions needed for the spectral weight integral I (Eq. 6).

3.2 Continuation of self energies, superconducting state

Our previous experience (8) is that in situations where a gap is present, continuation of the spectral function leads to unphysical broadening of the gap edge and that more accurate estimates can be obtained by continuing the self energy and then reconstructing the Green function from the Dyson equation. However, self energy continuation in the superconducting state is subject to complications.

Although analytical continuation of the anomalous self energy proceeds from Eq. 4, Σ_A'' is an odd function of frequency, so the issue of normalization must be handled differently. We rewrite the Kramers-Kronig relation in terms of $S = \Sigma_A''(\omega)/\omega$ as

$$\Sigma_A(i\omega_n) = \int \frac{dx}{\pi} \frac{xS(x)}{i\omega_n - x} \quad (5)$$

As Eq. 5 indicates, S is normalized to the zero frequency value of the anomalous self energy, which we obtain by a quadratic extrapolation of $1/\Sigma_A(i\omega_n)$ to $\omega_n = 0$. A very accurate extrapolation is needed because an incorrect normalization will lead to spurious features in the continued function, either very near zero or at high frequency.

The results of the continuation are shown in Fig. 2 and Fig 4. in the main paper. The upper panel of shows the imaginary parts of the normal and anomalous self energies obtained by separately continuing the Matsubara axis self energies obtained at $n = 1$ and $5.8t$. One sees that both the normal the self energies are dominated by poles at a low energy $\Omega_P^{N,A}$. The same

phenomena can be seen directly from the Matsubara axis data, without continuation. Fig. 3 shows the Matsubara axis frequency dependence of the anomalous term in the electron self energy. We see that the behavior is very close to the $\Sigma_A \sim 1/(\omega_n^2 + \omega_0^2)$.

In these continuations the pole strengths are comparable (integration, not shown, over the frequency range $0.1 < \omega < 0.2$ gives $0.32t^2$ for both curves) but we see that the pole positions are not quite identical $\Omega_P^N \neq \Omega_P^A$ and the widths are substantially different with the pole in the anomalous self energy being narrower. However, not all of the differences between the continued self energies are physical. In particular, the positivity of the density of states (imaginary part of trace of Nambu Green function) implies a delicate relation between the normal and anomalous self energies which may be violated by the inevitable errors of analytical continuation. In fact the density of states reconstructed from the self energies shown in Fig. 2 has an unphysical sign change in the vicinity of the pole frequency, arising mathematically from the slight difference in pole position combined with the relative narrowness of the peak in Σ_A'' . This problem does not occur in standard phonon-mediated superconductors because the pole strength in anomalous part of the self energy is small and the broadening is large.

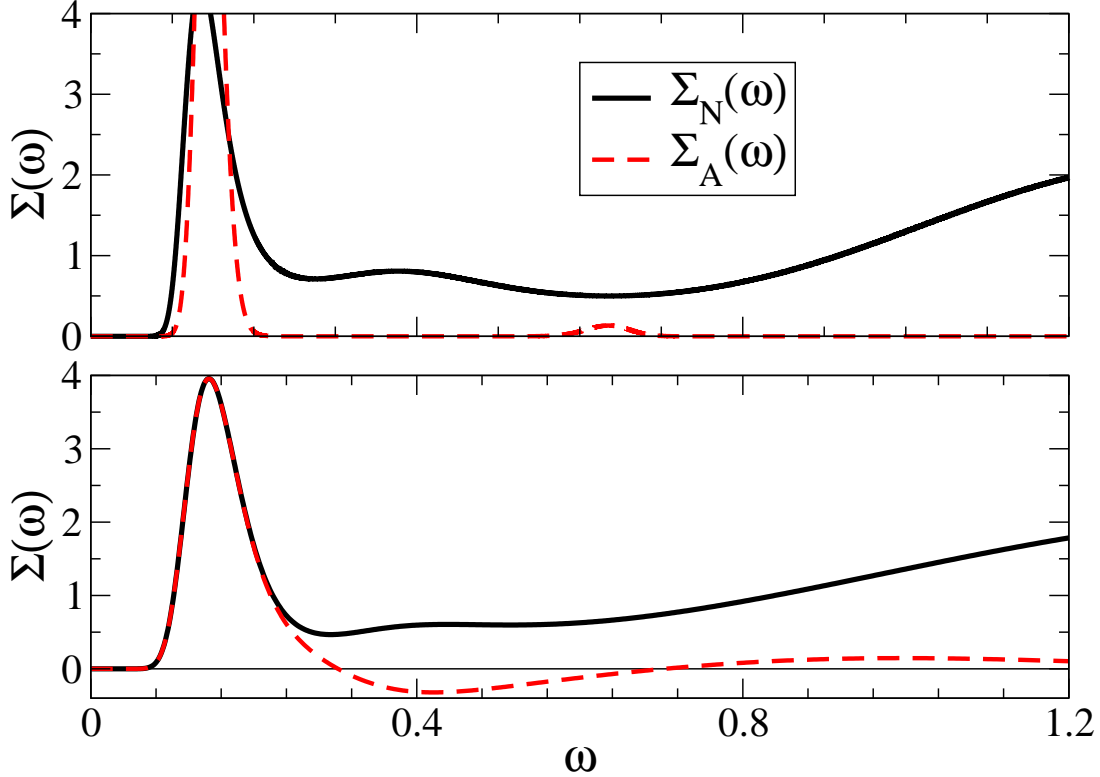


Figure 2: Imaginary part of the normal (τ_0 , black solid line) and anomalous (τ_1 , red dashed line) components of the self energy calculated for particle-hole symmetric Hubbard model at $n = 1$, $U = 5.8$, and $T = t/60$. Upper panel: self energies obtained by directly continuing Matsubara axis self energy. Lower panel: self energies obtained by continuing $\Sigma_{\pm} = \Sigma_N \pm \Sigma_A$

We have not found a reliable procedure for ensuring that analytical continuation of the self energies respects the relation between Σ_N and Σ_A implied by the positivity of the density of states, but in the particle-hole symmetric case (half filling, $t' = 0$) progress is possible because the Nambu Green function is diagonalized at all frequencies by the combinations $G_{\pm} = G_N \pm G_A$. In this case we continue $\Sigma_{\pm} = \Sigma_N \pm \Sigma_A$ and reconstruct the normal and anomalous components from the sum and difference. Results obtained for $n = 1$ and $U = 5.8t$ are shown in the lower panels of Fig. 2. At frequencies $\omega \gtrsim 0.2$, the inevitable errors in the continuations (in particular the small amplitude long period oscillations mentioned in the previous section) lead to a small unphysical (negative sign) component in Σ_A'' but the basic structure (a large pole at $\omega \sim 0.15t$) survives and the small negative values have a minimal effect on the resulting densities of states.

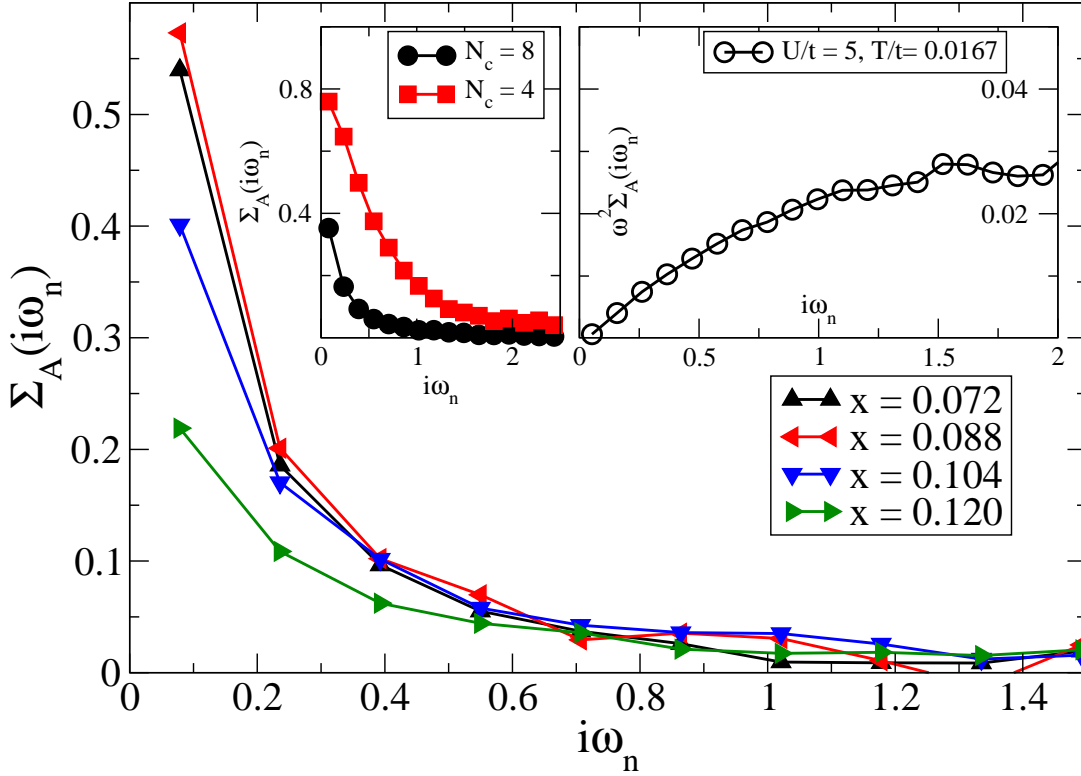


Figure 3: Main panel: frequency dependence of anomalous term in electron self energy computed for the 8-site DCA approximation at $T = t/40$, $U = 7t$, and densities indicated. Left inset: comparison of frequency dependence of anomalous self energy for 4 and 8-site cluster approximations computed at $U = 6t$, $T = t/40$ and $x = 0.08$. Right inset: product $\omega^2 \Sigma_A(i\omega_n)$ demonstrates $1/\omega_n^2$ decay of anomalous self energy for $U = 5t$ and $x = 0$.

4 Transfer of spectral weight between superconducting and normal states

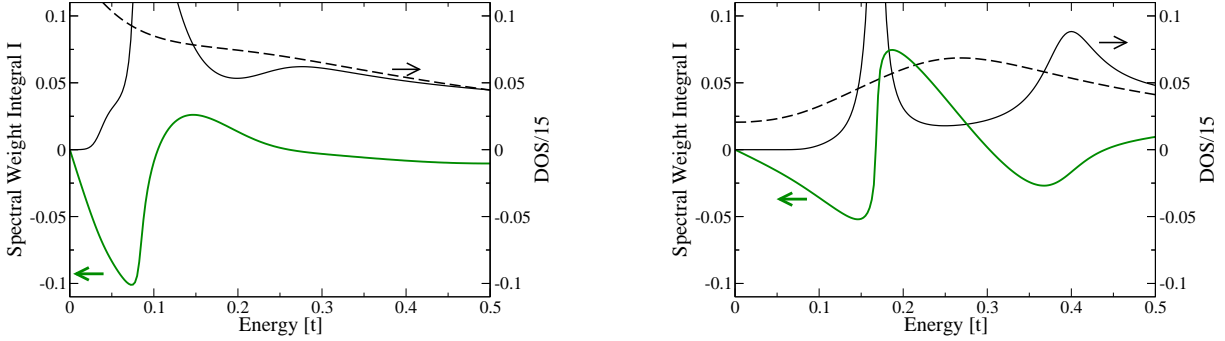


Figure 4: Heavy solid line (green online, left vertical axis): spectral weight transfer integral Eq. 6 computed as described in the text for $U = 5.0t$ (left panel) and $U = 5.8t$ (right panel). Light solid and dashed lines: superconducting and normal densities of states, divided by 15 so as to appear on the same scale.

Inspection of Fig. (3) of the main text suggests that when superconductivity emerges from a Fermi liquid state, the spectral weight in the superconducting coherence peak is transferred up from energies below the superconducting gap, whereas when superconductivity emerges from the pseudogap state the weight in the superconducting coherence peak is transferred down from higher energies. Making this statement more precise is difficult because in the general (non-particle-hole symmetric) case the magnitude of the weight transfer is close to the limits imposed by the uncertainties in our analytical continuations. However, the higher-precision data obtainable in the particle-hole symmetric case (which does not have a sign problem) along with the sharper spectra obtained by our ability to continue Σ_{\pm} in this case permits progress. We construct the real-axis $\Sigma_{N,A}$ from Σ_{\pm} for $n = 1$ and $U = 5.0$ (non-superconducting state is Fermi liquid) and $U = 5.8$ (non-superconducting state has a pseudogap) as described above, compute the Green function by inverting the Nambu-Dyson equation and then compute

$$I(\omega) = \int_0^{\omega} dx (\text{Im}G_S(x) - \text{Im}G_N(x)). \quad (6)$$

The long-period oscillations discussed above lead to an I which fluctuates between $\sim \pm 0.02$ for $\omega \gtrsim 0.4t$; values of $|I| < 0.02$ are thus indistinguishable from 0 within our accuracy.

The heavy solid line (left axis, green online) in the two panels of Figs. 4 shows the resulting I . In both cases, the difference is initially negative, reflecting the sharp gap in the superconducting state. At the gap onset the difference rises sharply, reflecting the weight in the superconducting coherence peak. In the left panel (overdoped case) the weight difference tends rapidly to zero as energy is raised above the gap energy, reflecting the fact that the weight in the

superconducting coherence peak is drawn mainly from states pushed up from low energy by the formation of the gap. In the right panel (underdoped case), the difference becomes strongly positive for a range of $\omega > \Delta$, illustrating the fact that in this case the superconducting coherence peak is formed in large part by pulling weight down from higher energy states. One sees that at higher frequencies I oscillates about zero. The difficulties discussed above set an absolute limit of about ± 0.02 on our ability to determine the difference: values smaller than this are not distinguishable from zero within our accuracy, so we believe that for frequencies bigger than about 3Δ the difference integral is zero within our errors.

References

1. T. Maier, M. Jarrell, T. Pruschke, M. H. Hettler, *Rev. Mod. Phys.* **77**, 1027 (2005).
2. B. Bauer, *et al.*, *Journal of Statistical Mechanics: Theory and Experiment* **2011**, P05001 (2011).
3. A. Albuquerque, F. Alet, P. Corboz, *et al.*, *J. Magn. Magn. Mater.* **310**, 1187 (2007).
4. E. Gull, *et al.*, *Computer Physics Communications* **182**, 1078 (2011).
5. E. Gull, *et al.*, *Phys. Rev. B* **83**, 075122 (2011).
6. M. Jarrell, J. E. Gubernatis, *Physics Reports* **269**, 133 (1996).
7. N. Lin, E. Gull, A. J. Millis, *Phys. Rev. B* **82**, 045104 (2010).
8. X. Wang, E. Gull, L. de' Medici, M. Capone, A. J. Millis, *Phys. Rev. B* **80**, 045101 (2009).